

Transient Magnetic and Doppler Features Related to the White-light Flares in NOAA 10486

R. A. Maurya¹ · A. Ambastha² ·

© Springer •••

Abstract Rapidly moving transient features have been detected in magnetic and Doppler images of super-active region NOAA 10486 during the X17/4B flare of October 28, 2003 and the X10/2B flare of October 29, 2003. Both these flares were extremely energetic white-light events. The transient features appeared during the impulsive phase of the flares, and moved with speeds ranging from 30 to 50 km/s. These features were located near the previously reported compact acoustic (Donea and Lindsey, 2005) and seismic sources (Zharkova and Zharkov, 2007). We examine origin of these features and their relationship with various observed aspects of the flares, *viz.*, RHESSI hard X-ray emission sources, and the flare-kernels at different layers - (i) photosphere (white-light continuum), (ii) chromosphere ($H\alpha$ 6563Å), (iii) temperature minimum region (UV 1600Å), and (iv) transition region (UV 284Å).

Keywords: Active Regions, Magnetic Fields; Active Regions, Velocity Field; Flares, Dynamics

1. Introduction

The catastrophic change in the magnetic field topology in the solar corona is believed to trigger energetic events, such as, solar flares and CMEs. This MHD catastrophe leads to the reconnection of magnetic field lines in the corona that results in a wealth of observed post-flare phenomena. As the flares derive their energy from magnetic field, it is expected that magnetic non-potentiality would relax toward a lower energy state after the excess energy available in the active region is released. It was first suggested several decades ago by Giovanelli (1939) that flares should be associated with magnetic field changes. Extensive efforts have been made since then to find such changes using photospheric magnetic field measured by ground-based observations (Patterson and Zirin, 1981; Patterson, 1984; Wang *et al.*, 1992; Ambastha, Hagyard, and West, 1993; Chen *et al.*, 1994);

¹Udaipur Solar Observatory (Physical Research Laboratory),
 P.O. Box 198, Dewali, Badi Road, Udaipur 313 001, INDIA.

¹ e.mail: ramajor@prl.res.in

² e.mail: ambastha@prl.res.in

Hagyard, Stark, and Venkatakrishnan, 1999), and more recently, by space-borne instruments (Kosovichev and Zharkova, 2001; Qiu and Gary, 2003; Wang, 2006).■

A wide variety of results have been reported on the pre- and post-flare changes in magnetic field parameters, that remained mostly unreliable because of poor sensitivity, spatial resolution, cadence, and coverage of the available magnetographs. Furthermore, serious questions have also been raised about the observed nature of magnetic field changes, as the measurements which generally employ some photospheric spectral lines are expected to be affected by flare-induced line profile changes (Harvey, 1986; Qiu and Gary, 2003). Nevertheless, with the availability of recent high-quality, high-cadence magnetic field observations, there has been mounting evidence of rapid, permanent changes in the longitudinal and transverse magnetic fields during the course of large flares (Sudol and Harvey, 2005).

There are some other physical processes accompanying the sudden energy release in the solar corona which may influence the magnetic field measurements. The flare energy release in the corona accelerates the charged particles, i.e., electrons and protons. A large number of these particles can precipitate along the magnetic field-lines and lose their energy in the lower atmosphere. During this process, microwave radiation is produced by a gyrosynchrotron process, and hard X-rays (HXR) emission through a thick-target bremsstrahlung process (Brown, 1971; Emslie, 1978). White-light flares (WLFs), the most energetic of all flares, were suggested to be associated with direct heating by nonthermal or accelerated particles, specifically quasi-relativistic electrons (Rust and Hegwer, 1975; Hudson *et al.*, 1992; Neidig and Kane, 1993). This is observationally supported by HXR footpoints, the site of nonthermal particle acceleration, matching well with the WLF ribbons; (Fletcher and Hudson, 2001; Metcalf *et al.*, 2003). However, only very high energy electrons, with energy exceeding a few MeV, are expected to penetrate to the deeper layers due to large photospheric density. It was inferred from the TRACE WL and Yohkoh/HXT data that WLF ribbons originate in the chromosphere and the temperature minimum region, and the enhanced WL emission is caused by ionization and subsequent recombination of hydrogen. Energy thus deposited in the chromosphere by the electron beam is then transported to the lower atmosphere by back-warming. The observed changes in magnetic fields during the impulsive phases of flares would be affected by a combination of these various effects.

During the impulsive phase of some flares, a localized sign reversal of magnetic polarity, termed as “magnetic anomaly”, has been observed (Qiu *et al.*, 2002; Qiu and Gary, 2003). Such sign reversal has also been attributed to the change in the line profile from absorption to emission by numerical models (Machado *et al.*, 1980; Vernazza, Avrett, and Loeser, 1981; Ding and Fang, 1989; Ding, Qiu, and Wang, 2002).■ However, non-LTE calculations for Ni I 6768Å, used for magnetic field measurements in GONG¹ and SOHO/MDI² instruments, have shown that this absorption line can turn into emission only if there is a strong rise in the electron density

¹Global Oscillation Network Group

²Solar and Heliospheric Observatory, Michelson Doppler Imager

near cooler area, i.e., sunspot umbra/penumbra, and not by heating of the atmosphere by any other means. Consistent with this result, Qiu and Gary (2003) discovered sign reversal in locations of strong HXR emission. Edelman *et al.* (2004) have also simulated the GONG and MDI observations for solar flares and concluded that the magnetic field measurement is less sensitive to the line shape changes, while velocity estimates strongly depend on line variations. In addition, their numerical simulation also showed that the observed transient sign reversal may be produced when the Ni I 6768Å line profile turns into emission as a result of non-thermal beam impact on the atmosphere in regions of strong magnetic fields. The effect of line profile changes on magnetic field estimates has also been reported by (Abramenko and Baranovsky, 2004). Injection and transport of high-energy electrons was observationally inferred from a M9.8 flare observed in microwave by Owens Valley Solar Array, and in HXR by hard X-ray telescope on board *Yohkoh* (Lee *et al.*, 2002).

More recently, flare-associated helioseismic effects have been reported using different local helioseismology techniques, e.g., acoustic sources detection by holography (Donea and Lindsey 2005), flare-induced seismic waves using time-distance analysis (Kosovichev, 2006), and post-flare amplitude enhancement of acoustic or p-modes by ring-diagram technique (Ambastha, Basu, and Antia, 2003; Ambastha *et al.*, 2004). Zharkova and Zharkov (2007) have found seismic sources to be located near the acoustic sources discovered by Donea and Lindsey (2005) during the large flare in NOAA 10486. Several flare productive regions have been extensively studied, including the super-active region NOAA 10486.

While examining the GONG magnetograms movies, obtained during the X17/4B flare of October 28, 2003 in NOAA 10486, rapidly “moving” magnetic transient features were detected around the impulsive phase of the flare (Ambastha, 2007; Maurya and Ambastha, 2008). This interesting transient feature moved away from the flare site with a velocity ≈ 40 km/s that was comparable to the velocity of seismic waves reported earlier by Kosovichev and Zharkova (1998). It does not appear to be an instrumental artifact as both the GONG and MDI movies exhibited this feature. The exact nature of the moving magnetic feature is not well understood, and requires further investigation. If the moving magnetic feature was indeed related to the white-light flare by way of the absorption line profile turning in to emission, it is expected to have a relationship with the white-light flare-kernels. In particular, it would also be interesting to examine whether this feature was essentially a “moving” sign-reversal anomaly associated with HXR sources produced by nonthermal electron beams (Qiu *et al.*, 2002). It is to note that “velocity transients” were also detected in the GONG (and MDI) dopplergrams during the impulsive phase of the flare. Earlier, Venkatakrishnan, Kumar, and Uddin (2008) also found localized velocity enhancements, co-spatial with H α flare-kernels, during this flare.

In this paper, we discuss the spatial and temporal correlation of the “moving” magnetic and velocity transient features (MFs) using MDI and GONG magnetograms and Dopplergrams, during the energetic white-light flares (WLFs) of October 28 and 29, 2003. We examine the properties of these MFs in the light of recent studies related to flare-associated changes in magnetic and velocity fields.

We also attempt to find their spatial and temporal correlation with the flare kernels as observed in the lower atmosphere, i.e. photosphere and chromosphere, and corresponding features in the upper layers using the available multi-wavelength observations. In Section 2, we describe the observational data used in this study. Technique of data analysis is given in Section 3. The properties of MFs and associated flare-kernels are described in Sections 4 - 5. Finally, discussions and conclusions are presented in Section 6.

2. The observational data

We have used magnetograms, Dopplergrams and white-light images obtained by GONG and SOHO/MDI to study the flares of October 28 and 29, 2003. These observations provide information on the temporal and spatial evolution of photospheric magnetic field, velocity field and intensity in NOAA 10486. To examine the properties of the magnetic and Doppler MFs, and their correlation with the flare-kernels, we have used white-light intensity images for the photospheric layer. For upper atmospheric layers, we have used TRACE³ UV 1600Å for the temperature minimum region, chromospheric H α observations obtained from USO⁴ and MLSO⁵, and TRACE UV 284Å for the transition region. To compare the locations of flare kernels and MFs with HXR sources, we have used HXR data obtained by RHESSI⁶. These observations are described below:

- **GONG data:** The magnetograms, Dopplergrams and white-light images obtained from GONG instrument have spatial and temporal resolutions of 2.5 arc-sec/pixel and 1 minute, respectively (Harvey *et al.*, 1988). The instrument uses Ni I line centered at 6768Å, and works on the principle of phase shift interferometry (Harvey 2008, private communication, also see Appendix).
- **SOHO/MDI data:** In addition to the GONG data, we have also used the corresponding SOHO/MDI data (Scherrer *et al.*, 1995), to inter-compare the observed changes in magnetic, velocity and intensity maps. The SOHO/MDI data have spatial resolution of 2.0 arcsec/pixel and temporal cadence of 1 minute. (For a brief description of the observing principle, see Appendix).
- **USO H α :** We have used high spatial and temporal resolution H α filtergrams obtained from USO, Udaipur (India) for studying the chromospheric evolution of the X17/4B flare of October 28, 2003. These filtergrams were taken by a 15-cm aperture f/15 Spar telescope at a cadence of 30 sec during the quiet phase, and 3 sec in flare mode. The spatial resolution of USO filtergrams is 0.4 arcsec-per-pixel at the CCD detector plane.

³Transition Region and Coronal Explorer

⁴Udaipur Solar Observatory

⁵Mauna Loa Solar Observatory

⁶Reuven Ramaty High-Energy Solar Spectroscopic Imager

- **MLSO H α :** MLSO H α observations have been used for the October 29, 2003/20:49 UT X10/2B flare event as this flare occurred during the night-time of the USO, Udaipur site. This data has spatial and temporal resolution of 2.9 arcsec-per-pixel and 3 minutes, respectively.
- **TRACE UV:** The data corresponding to the temperature minimum and transition region were obtained from TRACE (Handy *et al.*, 1999; Schrijver *et al.*, 1999), which correspond to 1600Å and 284Å data sets, respectively. These images have spatial and temporal resolution of the order of 0.5 arcsec-per-pixel and 35 sec, respectively.
- **Hard X-ray:** We have used X-ray data obtained from RHESSI (Lin *et al.*, 2002), which observes solar HXR and γ -rays from 3 keV to 17 MeV with spatial resolution as high as \sim 2.3 arc-sec with a full-Sun field of view. The raw format data (i.e., modulated Fourier components) for both events were obtained from the RHESSI data site. HXR maps for the events were then constructed using Pixon method (Hurford *et al.*, 2002) under SolarSoft(SSW) for the dimension of 64×64 pixels centered at the flaring regions. The pixel resolution was 4 arc-sec and cadence was 1 minute. We chose different energy bands for the two flares due to their differing energetics: higher energy (100-200 keV) for the October 28, 2003 event and the lower energy (50-100 keV) for the October 29, 2003 event.

3. Data Analysis

To identify various features of interest during the evolution of the flares, we used time-series of full-disk magnetogram and Dopplergram images. Full disk images were aligned by de-rotating with the solar rotation. The areas-of-interest containing the active region NOAA 10486, where the flares of October 28 and 29, 2003 occurred, were selected from the de-rotated full disk images. We ignored the effect of solar differential rotation while correcting the images, since (i) the active region was located close to the solar equator, (ii) the selected area-of-interest was much smaller than the whole disk, and (iii) the duration of the flare-events was relatively short (\approx 15 minutes only).

We applied a Fourier technique based cross-correlation method to get co-aligned magnetograms registration within a sub-pixel accuracy. All the images were aligned using this procedure. To identify and select the corresponding areas-of-interest on various observational images, we overlaid the contours of magnetic flux. Then, by visual inspection of various structures, such as, filaments, sunspots and the overlying contours, we selected areas-of-interest from the corresponding images obtained by different instruments. Figures 1 and 8 show the selected areas of NOAA 10486 from TRACE UV 1600Å, USO H α , TRACE UV 284Å, MDI magnetogram/Dopplergram, and GONG white-light images, for the flares of October 28 and 29, 2003, respectively.

4. The X17/4B Flare of October 28, 2003/11:10 UT

The two-ribbon X17/4B flare of October 28, 2003, was one of the most energetic events that occurred in NOAA 10486. The active region was located close to the

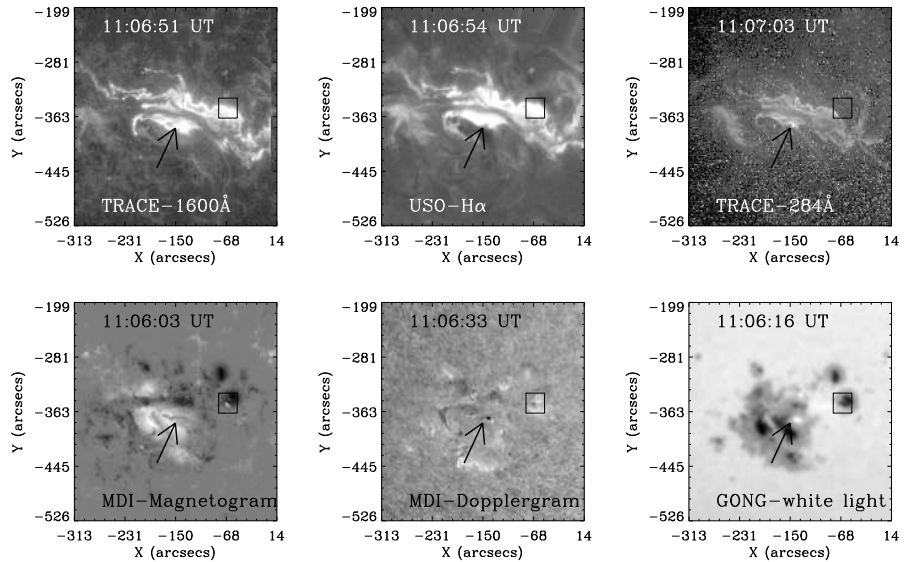


Figure 1. TRACE 1600Å, USO H α and TRACE 284Å (top row, from left to the right), and the MDI magnetogram, Dopplergram and GONG white-light image (bottom row, from left to the right) obtained around the peak phase of the white-light flare (X17/4B) of October 28, 2003. The arrows show the locations of the observed “moving” magnetic transient.

solar disk center at the time of this flare, therefore, projection effects did not pose any serious difficulty in the analysis. According to GOES⁷ X-ray flux data, this flare started at 09:51 UT and ended at 11:24 UT, with the maximum phase at 11:10 UT. However, the flare lasted considerably longer as seen in H α .

Significant changes were observed in the photospheric magnetic and velocity fields as seen from the movies of GONG and MDI observations for October 28, 2003. These included the gradual, evolutionary changes as the active region evolved during the course of the day. In addition, there were also abrupt and persistence changes, which occurred at some localized sites in the neighbourhood of the observed flare-kernels in white-light (Ambastha, 2007). Figure 1 shows multi-wavelength observations of this flare obtained during its peak phase corresponding to different layers of solar atmosphere. The top row shows the flare-kernels observed in the transition region, the chromosphere, and the temperature minimum region (from right to the left columns). It may be noted that the flare-kernels display structural similarity in these layers. The images corresponding to the photospheric level are shown in the bottom row: MDI magnetogram, MDI Dopplergram and GONG white-light (from left to the right columns). The white-light image clearly shows the emission kernels of this energetic WLF.

From the movies of GONG+ magnetogram images obtained during this super-flare, an interesting “magnetic” transient feature was also observed moving

⁷Geostationary Operational Environmental Satellite

rapidly away from the flare site around the magnetic neutral line. A portion of the feature was observed moving away from the neutral line toward the leading sunspot and the other perpendicular to it. These locations are marked by the arrow, and a rectangular box near the leading sunspot (Figure 1). These features appeared and faded in a few minutes' period during the impulsive phase of the flare (Ambastha, 2007; Ambastha, 2008; Maurya and Ambastha, 2008). Both GONG and MDI images exhibited these moving features. Similar, albeit fainter, velocity transients associated with the WLF event were also detected in the dopplergrams.

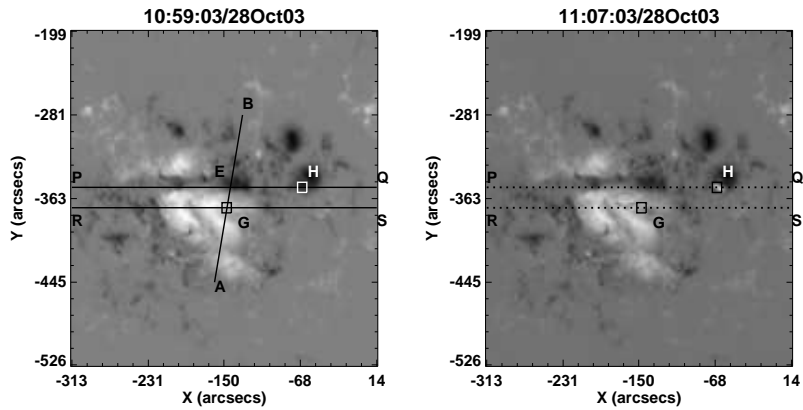


Figure 2. MDI magnetograms of NOAA 10486 taken around the pre- and peak phase of the October 28, 2003 flare at 10:59:03 UT (left panel), and 11:07:03 UT (right panel), respectively. Magnetic flux profiles along the lines PQ and RS are drawn in Figure 3. Here AB marks the direction of motion of the WLF kernels and the MFs, and the distances are estimated from a reference point E (left panel).

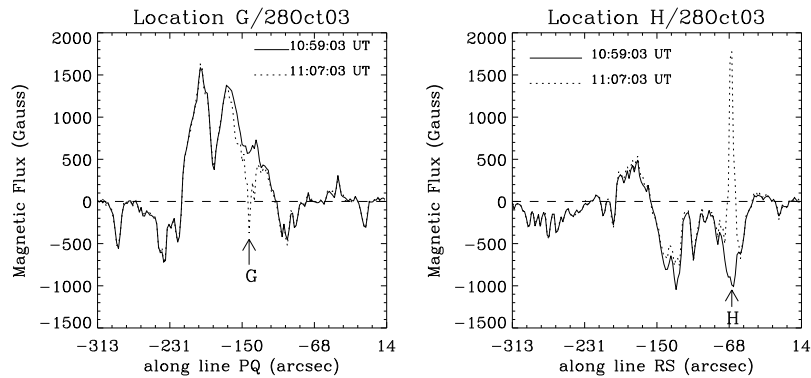


Figure 3. Magnetic flux profiles along PQ (left panel) and RS (right panel) as drawn in Figure 2. The solid and dotted lines represent the magnetic flux observed at 10:59:03 UT and 11:07:03 UT, respectively. Polarity reversals at points G and H are evident at the peak phase of the flare, i.e., 11:07:03 UT. Elsewhere along the lines, flux remained nearly unchanged.

4.1. Magnetic Field Transients and the Polarity Sign Reversal

Corresponding to the observed moving transients, we noticed a sign reversal of magnetic polarity (also, Doppler velocity) at some locations during the impulsive phase of the flare. To precisely identify the locations of sign reversal, we plotted magnetic flux profiles along a horizontal line moving from the bottom to the top of the selected magnetograms during the pre- and peak-phase of the flare. We found two locations G and H around which magnetic polarity sign reversal occurred (Figure 2). We have drawn reference lines PQ and RS passing through these two points over the magnetograms at 10:59:03 UT (solid lines) and 11:07:03 UT (dotted lines), respectively. The corresponding magnetic flux profiles along these lines are shown in Figure 3. It is evident that there are magnetic polarity reversals at G and H as the moving “magnetic” features passed over these locations at 11:07:03 UT. Else where, magnetic flux matched fairly well along the two lines at the two time instants.

Such sign reversals were already reported several years ago for some large flares by Zirin and Tanaka (1981). This was attributed to the heating of the lower atmosphere by the flare such that the core of the absorption line, used for measurement, turned to emission (Patterson, 1984). More recently, this effect was reported for the large X-class flare of April 6, 2001 using MDI magnetograms (Qiu and Gary, 2003). However, the sign reversal observed by MDI instrument is difficult to be explained by the sudden heating of the lower atmosphere. This is because Ni I 6768Å line (used by MDI and GONG instruments) is formed in the temperature minimum region and is rather stable against temperature changes (Bruls, 1993). Interestingly, Qiu and Gary (2003) noted that the sign-reversal occurred in the cooler umbral region of strong magnetic fields that was exactly co-aligned with HXR sources. This suggested that the sign reversal anomaly was associated with non-thermal electron beam precipitating to the lower atmosphere near the cool sunspot. This observation was further supported by a numerical simulation of the MDI measurements incorporating the flare effects.

The transient sign-reversals observed during the impulsive phase of the X17/4B flare in NOAA 10486 appears to be similar in nature as reported by Qiu and Gary (2003). However, in this case we found two locations that somewhat differed in their basic nature- (i) the sign reversal at H was located in the strong magnetic field of the leading, negative polarity umbra; similar to that reported by Qiu and Gary (2003), and was nearly stationary during the impulsive phase, (ii) the sign reversal at G first appeared near the neutral line at weak field location, and subsequently moved rapidly toward the stronger field regions of the positive polarity, following sunspots.

In the following section, we examine these features and their association with the flare-kernels observed at various solar atmospheric layers.

4.2. Motion of the Magnetic/Velocity Transients and Flare-kernels

On a visual inspection of the magnetograms/Dopplergrams and the filtergrams of the active region taken at various wavelengths, the magnetic transients appeared to be spatially correlated with the flare-kernels. For establishing this association

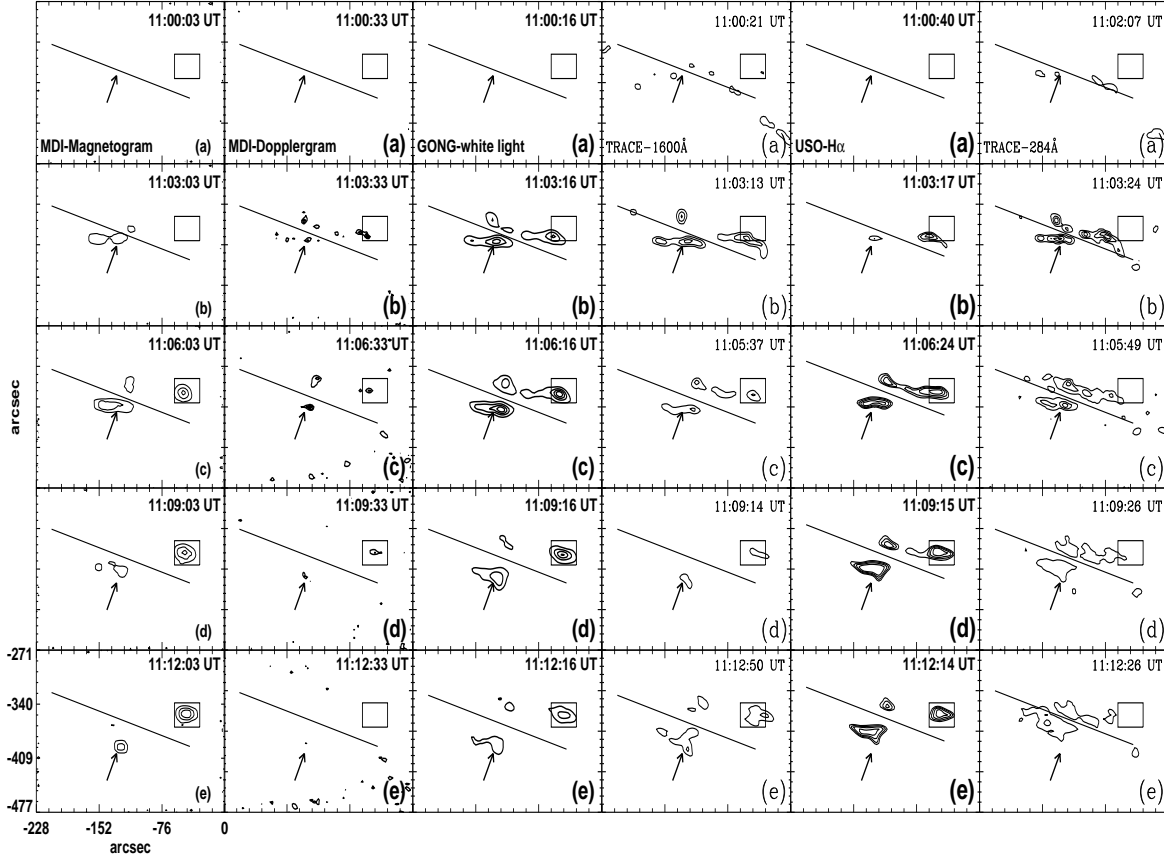


Figure 4. A mosaic of various observations obtained with time during the impulsive phase of the super-flare of October 28, 2003: MDI magnetograms, MDI Dopplergrams, GONG white-light, TRACE 1600Å, USO H α and TRACE 284Å (from left to the right columns). Appropriate contours (at 20, 40, 60 and 80% levels of the maximum values in the enhanced images) are shown corresponding to the magnetic/velocity transients and flare-kernels. Arrows and rectangular boxes mark the two locations of the moving transients.

further, we enhanced the transients using maximum entropy method (MEM) (Skilling and Bryan, 1984; Narayan and Nityananda, 1986). It is a deconvolution algorithm which operates by minimizing a smoothness function (“entropy”) in an image. Before applying this tool for each type of the observation, we subtracted the square root of a reference image from the square root of corresponding images obtained at different instants of time. Figure 4 (a-e) shows contours of suitably enhanced features observed during the impulsive phase of the flare in different sets of images, i.e., MDI magnetograms & dopplergrams, GONG white-light, TRACE 1600Å, USO H α and TRACE 284Å (from left to the right). These contours display the spatial and temporal evolution of the magnetic/velocity transients and flare-kernels observed at various atmospheric layers with increasing height, from the photosphere to the transition region. The selected contour levels correspond to 20, 40, 60 and 80% of maximum values of the enhanced images. The solid line in the figure represents an arbitrary reference line, RS, drawn along the neutral line, with respect to which the distances of various features are measured (*cf.*, Figure 2).

It is evident that the magnetic/velocity transients and the flare-kernels separated away from the reference neutral line with time during the impulsive phase of the flare (rows a-e, in each column). This follows the usual behaviour of two-ribbon flares. We also note that the evolution of magnetic transients (column 1) is spatially and temporally well correlated with the flare-kernels observed in different layers (columns 3-6). The locations of observed transients are marked by arrows and boxes in each frame. Along with the magnetic transients, comparatively fainter Doppler transients are also discernible during this period (column 2). These are similar to the Doppler-ribbons reported by Venkatakrishnan, Kumar, and Uddin (2008). The magnetic and velocity transients are observed to be particularly well correlated with the white-light kernels observed during the impulsive phase of the flare.

In order to quantitatively examine the motion of the observed features, we carried out the following procedure. Positions of transients and flare-kernels were measured from a reference point E (Figure 2, *left panel*) using an automatic algorithm implemented in IDL (Interactive Data Language). We followed the maximum value along the line EA, i.e., the direction of motion of the features, in the enhanced images obtained from MEM. The distance between the point of maximum value within a given feature (say E': x_1, y_1) and the reference point E (x_2, y_2), was calculated in pixels, using $d = [(x_2 - x_1)^2 + (y_2 - y_1)^2]^{1/2}$. This was then converted in kilometers using the pixel resolution of the corresponding instrument (Table 1).

From Figure 5, it is evident that magnetic/velocity transients and flare-kernels separated away during the impulsive phase of the X17/4B flare, i.e., 11:00 - 11:15 UT. Their distances from the reference point E along AB increased rapidly during the initial phase, i.e., 11:00-11:10 UT as seen in each row (corresponding to different observations) in the left column of the Figure. Thereafter, the rate of increase of separation slowed down. Table 1 shows an interesting trend in the maximum separation attained for the flare-kernels: it was the shortest, i.e., ≈ 15 Mm at the transition layer observed in UV 284Å (TRACE). Moving downwards to the lower layers, it increased to ≈ 20 Mm at the chromosphere (USO-H α)

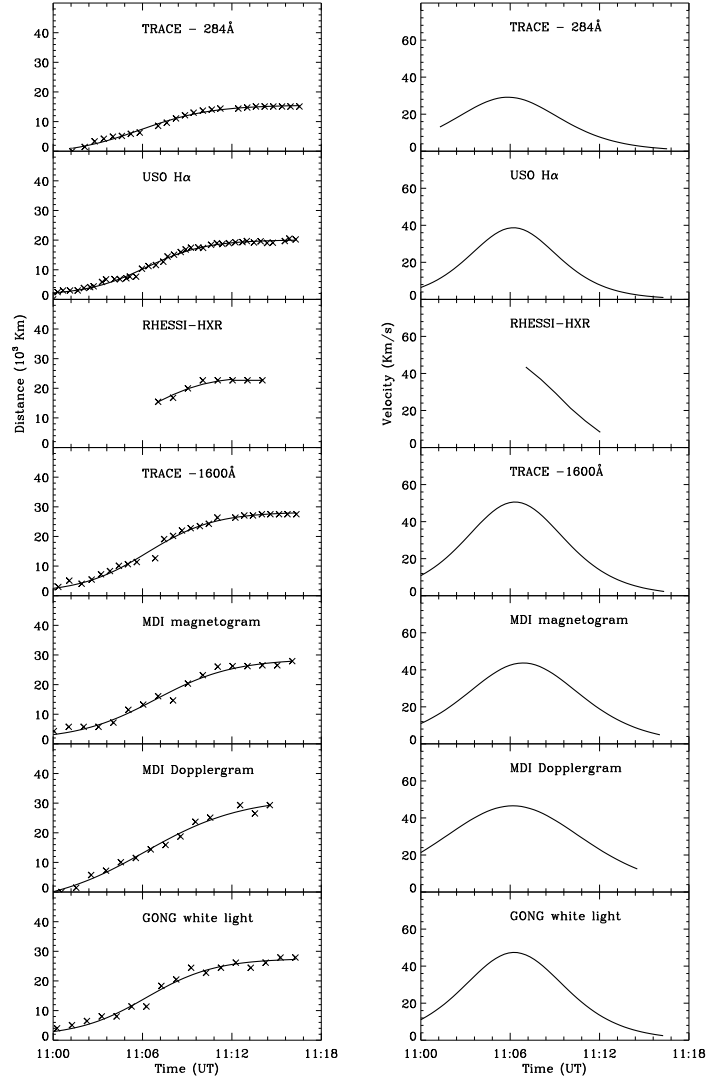


Figure 5. *Left Panel:* Distances of flare-kernels and magnetic/doppler transients from a reference line during 11:00-11:15 UT using different observations: TRACE 284Å, H α , TRACE 1600Å, RHESSI-HXR, magnetogram, Dopplergram and white-light (from top to the bottom rows). The measured distances are marked by “x”, while, the solid profiles represent the Boltzmann sigmoid fitting through these points. *Right Panel:* Separation velocities derived for various features from the fitted distances corresponding to the *left panel*.

Table 1. Maximum distances, velocities, and time at the maximum velocities of transients.

S.N.	Data	Pixel Res. (arcsec)	Layer	Max. Dist. (Mm)	Max. Vel. (km s ⁻¹)	Time of Max. Vel. (UT)
1	TRACE 284Å	0.5	TR ¹	15.4±0.3	29±4	11:05:40
2	USO-H α	0.4	Chr ²	20.0±0.3	38±5	11:06:20
3	HXR	4.0	Chr ²	23.1±0.8	43±9	11:07:03
4	TRACE 1600Å	0.5	TM ³	28.0±0.3	50±7	11:06:13
5	GONG WL	2.5	Pho ⁴	27.3±0.5	45±6	11:06:10
6	MDI Dopper	2.0	Pho ⁴	29.3±0.5	46±5	11:06:10
7	MDI Magneto	2.0	Pho ⁴	27.9±0.4	43±4	11:06:49

¹TR: Transition Region, ²Chr: Chromosphere,³TM: Temperature Minimum, ⁴Pho: Photosphere

and ≈ 28 Mm in the temperature minimum region and the photosphere (UV 1600Å TRACE, and GONG & MDI photospheric data). This trend is consistent with the classical flare model of an expanding loop structure with foot-points anchored in the lower atmosphere. The HXR feature also showed separation of ≈ 23 Mm, closer to the separation observed in chromospheric H α . This is consistent with the formation of HXR sources some where in the lower chromospheric layer. The magnetic and doppler transients, on the other hand, showed a larger separation of $\approx 29 Mm$, closer to the value obtained for the photospheric WLF kernels.

We derived the relative velocities of various features moving along the direction AB, away from the reference line RS, by fitting a Boltzmann sigmoid (best fitting) to the observed positions. This is given by

$$d(t) = A_0 + \frac{A_1 - A_0}{1 + e^{(t - A_2)/A_3}}$$

where, A_0, A_1, A_2 and A_3 are fitting parameters; A_0 - top (i.e., maximum of $d(t)$), A_1 - bottom (i.e., minimum of $d(t)$), A_2 - the time at which distance is halfway between bottom and top, and A_3 - the steepness of the curve, with a larger value denoting a shallower curve.

The velocity $v(t)$ is then obtained by taking the time derivative of the fitted distance function $d(t)$. Figure 5 shows the fitted distances (solid curves) passing through the measured distances marked by “ \times ” symbols (*left panel*), and the derived velocities (*right panel*). Velocities of flare-kernels and the magnetic/Doppler transient features reached a peak (or maximum) around 11:06 UT. It is also clear from this figure and Table 1 that the flare-kernels separated faster with velocity of 45-50 km/s in the lower atmosphere, i.e., the temperature minimum region and the photosphere, as compared to that in the upper atmosphere, i.e., 38 km/s at the chromosphere, and 29 km/sec at the even higher transition region.

It is known that the systematic separation of H α flare-kernels is the chromospheric signature of magnetic reconnection process progressively occurring at

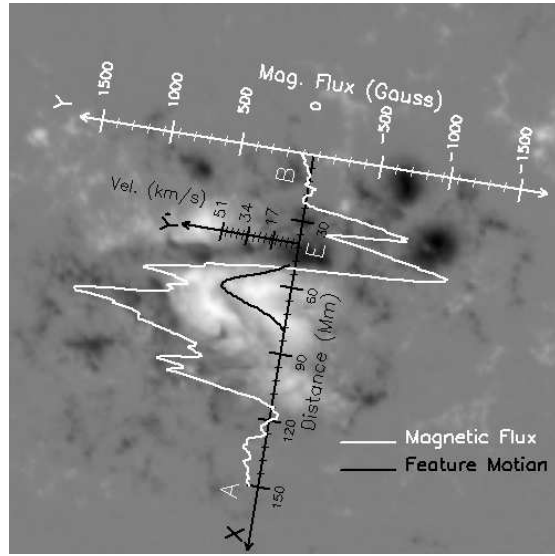


Figure 6. Velocity profile of the moving "magnetic" feature (dark) measured along the reference line BA overlaid on the MDI magnetogram (background half-tone image). The magnetic flux variation along the trajectory of motion of the feature is drawn as white profile.

higher levels in the corona. Rather smaller separation velocity in the range of $\approx 3\text{-}10$ km/s have been reported for two-ribbon flares associated with filament eruptions, as compared to the velocities in the range of 30–50 km/s obtained for the flares in NOAA 10486 (Table 1). However, it is noted that larger separation velocities in the range 20–100 km/s have also been reported during some recent two-ribbon flares, particularly those occurring in complex active regions (Qiu *et al.*, 2002). As the flare-ribbons encounter regions of stronger magnetic fields, their speeds are known to decrease. A similar behaviour is observed for the moving magnetic transient as well as the flare kernels corresponding to the flare of October 28, 2003. Figure 6 shows the velocity profile (dark curve) of the moving magnetic feature from the neutral line along the direction marked by the line BA. It is clear that its velocity initially increased with the magnetic flux (white curve), attained a peak value, then decreased and vanished close to the location where the magnetic flux attained a maximum value. This is consistent with the general observation for flare-ribbons moving toward strong magnetic field regions.

4.3. RHESSI Hard X-ray Sources and the White-light Flare of October 28, 2003

Figure 7 shows the temporal and spatial evolution of the enhanced white-light flare-kernels (red patches) observed in the GONG intensity maps (green half-tone images) obtained during the impulsive phase of the X17/4B flare of October 28, 2003 (top rows 1-2). Similarly, evolution of the moving magnetic transients (magenta patches) are shown over the same background images in the bottom rows (3-4). White contours represent the RHESSI HXR flux in the energy range

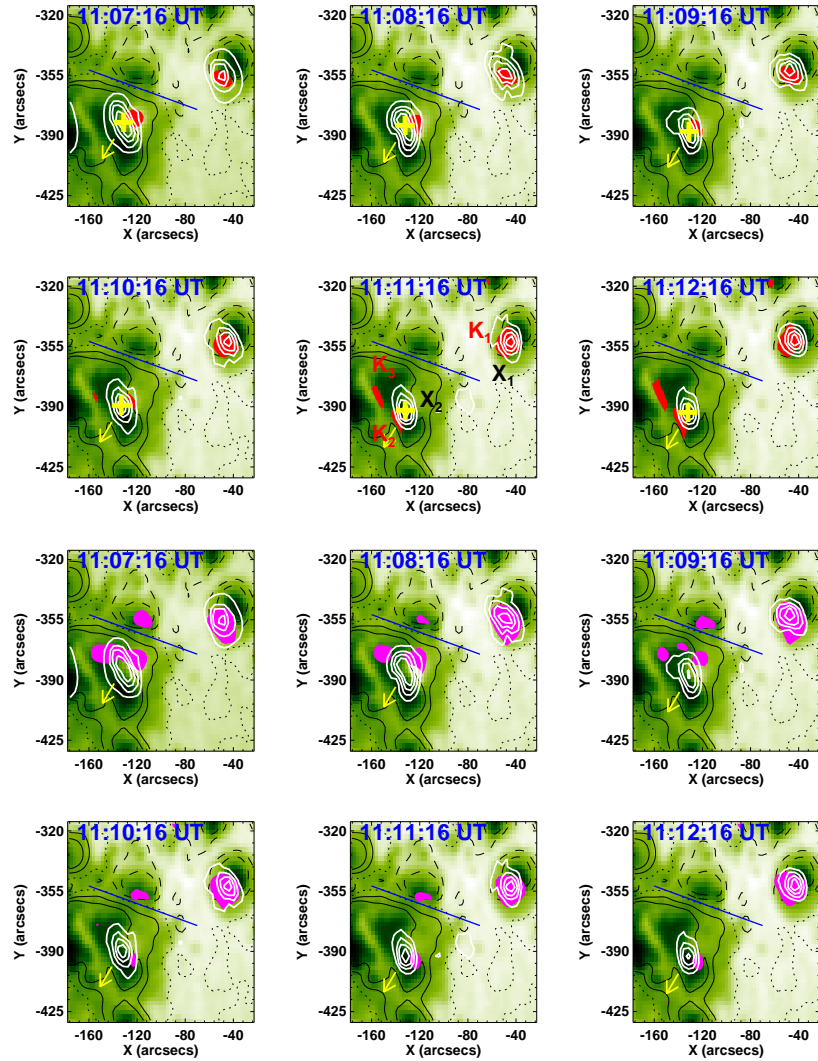


Figure 7. Time-sequence of white-light intensity maps (background green half-tone image) during the impulsive phase of the X17/4B flare - 11:07:16-11:12:16 UT on October 28, 2003. Superimposed dashed (solid) contours represent negative (positive) flux at $\pm 800, \pm 1500$ gauss levels, while the dotted contours mark the magnetic neutral lines. RHESSI hard X-ray fluxes (white contours) in the energy range 100–200 keV are overlaid at the levels 20, 40, 60, 80% of the maximum value. The red patches mark the enhanced WLF kernels (top rows 1-2), and the magenta patches represent the enhanced magnetic transients (bottom rows 3-4).

100–200 keV associated with the flare during its impulsive phase, i.e., 11:07:03–11:12:03 UT, at 20, 40, 60, 80% levels of the maximum HXR flux. The central maxima of the hard X-ray source (marked by “+” sign in yellow color) was found to be moving, in the direction of the arrow, with a velocity of 43 km/s from the reference line, i.e., the solid blue line drawn along the neutral line. Velocity of the

HXR feature was similar to that of the moving magnetic/velocity transient and the white-light flare-kernels (cf., Table 1), however, their relative spatial positions differed to some extent. HXR features were earlier reported to form during the impulsive phase of an X5.6 flare of April 6, 2001 in strong magnetic fields of the order $\pm 1000\text{-}1500$ G (Qiu and Gary, 2003). Figure 4 shows that the moving magnetic transient, where sign reversal occurred, first appeared around 11:03 UT very close to the neutral line, i.e., at a weak magnetic field location. Thereafter, it moved towards the direction of strong magnetic field of the following (positive) polarity umbra. Unfortunately, we do not have the entire temporal sequence in RHESSI HXR due to the non-availability of data before 11:07:16 UT, therefore, it is not clear whether HXR source also initially formed near the neutral line.

Qiu and Gary (2003) noted that the locations of sign-reversal “anomaly” coincided well with the locations of the HXR foot-points. They suggested the observed anomalous magnetic features to be related to electron precipitation into the lower atmosphere, but not with all white-light kernels. They gave the energetics for the reversal of line-profiles in the umbral, i.e., strong magnetic field and cooler regions, as compared to that in the relatively hotter locations of weaker magnetic field area. In this case, in agreement with Qiu and Gary (2003), we observed that HXR foot-point X1 formed at the locations of strong field of the leading umbra. This HXR source X1 was nearly stationary, and matched well with the WLF kernel K1 (rows 1-2), and also the magnetic transient observed over the leading sunspot (rows 3-4). However, the WLF kernel did not match well with the HXR-maximum at X2. It is observed that the WLF kernel K2 first appeared at one edge of X2 contours (11:07:16 UT), then decayed and appeared at the opposite edge (11:11:16 UT). Around the same time, WLF kernel K3 appeared that was not associated with any HXR feature. The association of the moving magnetic features at X2 appeared to better than the WLF kernels. Thus, the association of HXR source with the anomalous magnetic polarity feature as reported by Qiu and Gary (2003) does appear to hold in this case.

5. The X10/2B Flare of October 29, 2003/20:49 UT

This white-light flare, classified as X10/2B (from GOES-10), occurred in active region NOAA 10486 on the following day of the X17/4B flare, i.e., on October 29, 2003. It was located still closer to the disk center at S15W02. The flare began at 20:37 UT, reached peak phase at 20:49 UT, and decayed at 21:01 UT. Figure 8 shows a mosaic of the flare as observed in the TRACE 1600Å, H α and TRACE 284Å (top row). The photospheric magnetogram, Dopplergram and white-light images are shown in the bottom row. As detected during the white-light flare of October 28, 2003, we found moving transient features around the impulsive phase of this energetic event also. However, this event was located in a different part of the active region from the event of October 28, 2003. The magnetic transients and WLF kernels are marked by arrows in each frame of Figure 8. The characteristics of the MFs and flare-kernels are described in the following sections.

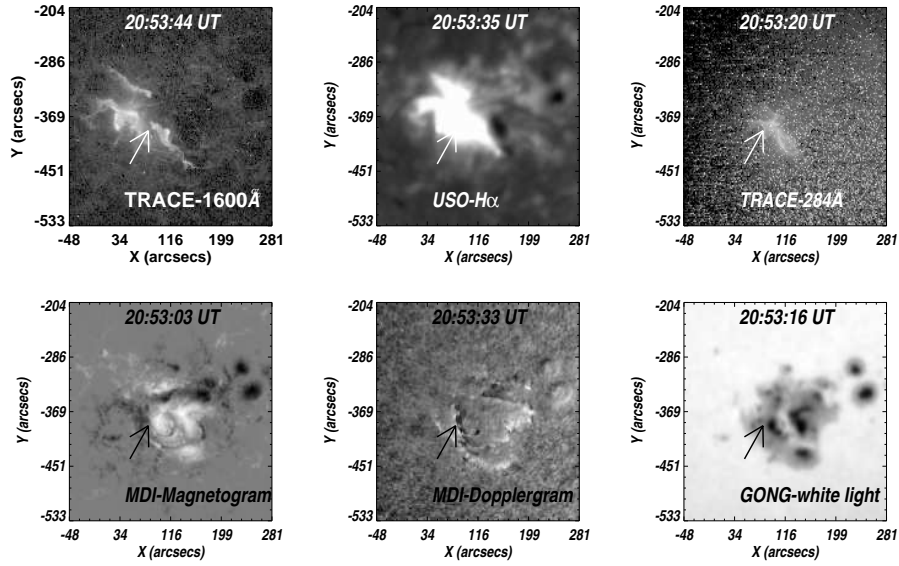


Figure 8. TRACE 1600Å, MLSO H α and TRACE 284Å (top row, from left to the right) and the MDI magnetogram, Dopplergram and GONG white-light image (bottom row, from left to the right) obtained during the peak phase of the white-light flare (X10/2B) of October 29, 2003. The arrow shows the location of “moving” magnetic transient.

5.1. Magnetic Field Transients and the Sign Reversal

Magnetogram movies were used to detect magnetic transients during the impulsive phase of this flare also (cf., Figure 9). We identified the locations B and C of polarity sign reversals that occurred at 20:42:03 UT. This was done by displaying magnetic flux along a horizontal line which was moved from the bottom to the top of magnetograms selected during the pre-peak and peak phases of the flare. The magnetic flux along XY and LM is plotted in Figure 10. The solid and dotted lines in the figure correspond to the time of pre-peak phase (20:36:03 UT) and the peak phase (20:42:03 UT), respectively. It is observed that the magnetic flux changed sign around B and C. Else where along the lines XY and LM, the magnetic flux remained nearly unchanged.

5.2. Motion of the magnetic/velocity transients and flare-kernels

A careful examination of the movies of MDI magnetograms and Dopplergrams of the October 29, 2003 event revealed moving magnetic and velocity features along with the flare-kernels during the impulsive phase. The spatial and temporal evolution of the MFs and flare-kernels observed during this event are illustrated in Figure 11. The contours levels were derived from the same technique (MEM) as used for the previous event of October 28, 2003. Different observations from the photospheric magnetograms MDI), Dopplergrams (MDI) and white-light (GONG) to chromospheric H α (MLSO) through temperature

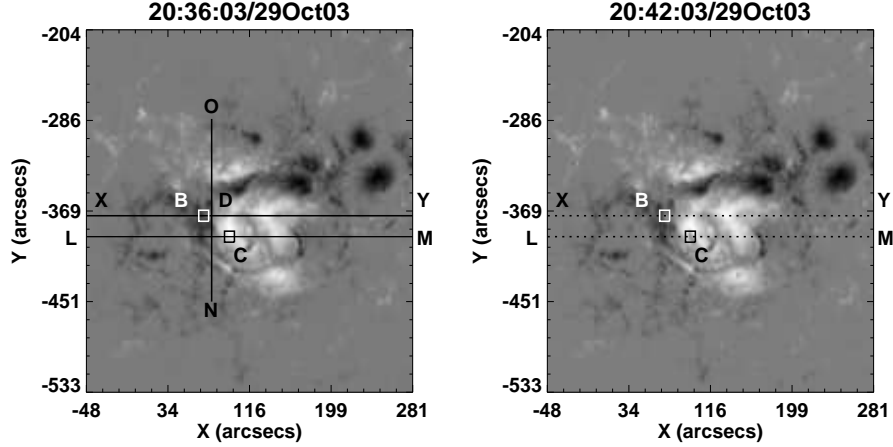


Figure 9. MDI magnetograms of NOAA 10486 taken around the pre- and peak phase of the October 29, 2003 flare at 20:36:03 UT (left panel), and 20:42:03 UT (Right Panel), respectively. Magnetic flux along the lines XY and LM is drawn in Figure 10. Sign reversal in flux polarity was detected at “B” and “C” across the neutral line. The reference point “D” on the vertical line NO represents the point from which the distances of flare kernels are measured along line DX.

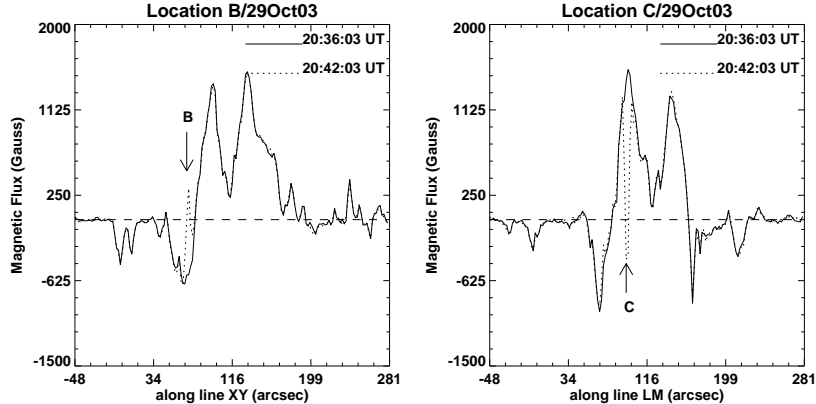


Figure 10. Magnetic flux profiles along the lines XY and LM (as drawn in Figure 9). The solid and dotted lines represent the magnetic flux values obtained at 20:36:03UT and 20:42:03 UT, respectively. Polarity sign reversals are evident at the locations B and C marked in Figure 9, during the peak phase of the white-light flare at 20:42:03 UT, while, the flux remained nearly unchanged else where along the lines XY and LM.

minimum UV-1600Å(TRACE) are shown from the left to the right column. The MFs appeared to be correlated with the flare-kernels observed in the white-light and other wavelengths corresponding to various layers of solar atmosphere. The temporal evolution of MFs and flare kernels are given from the top (a) to the bottom (e) rows in each column. A solid line, drawn in each frame, marks the reference direction perpendicular to which MFs and flare kernels moved away. The solid arrow shows the locations of the MFs in different sets of images.

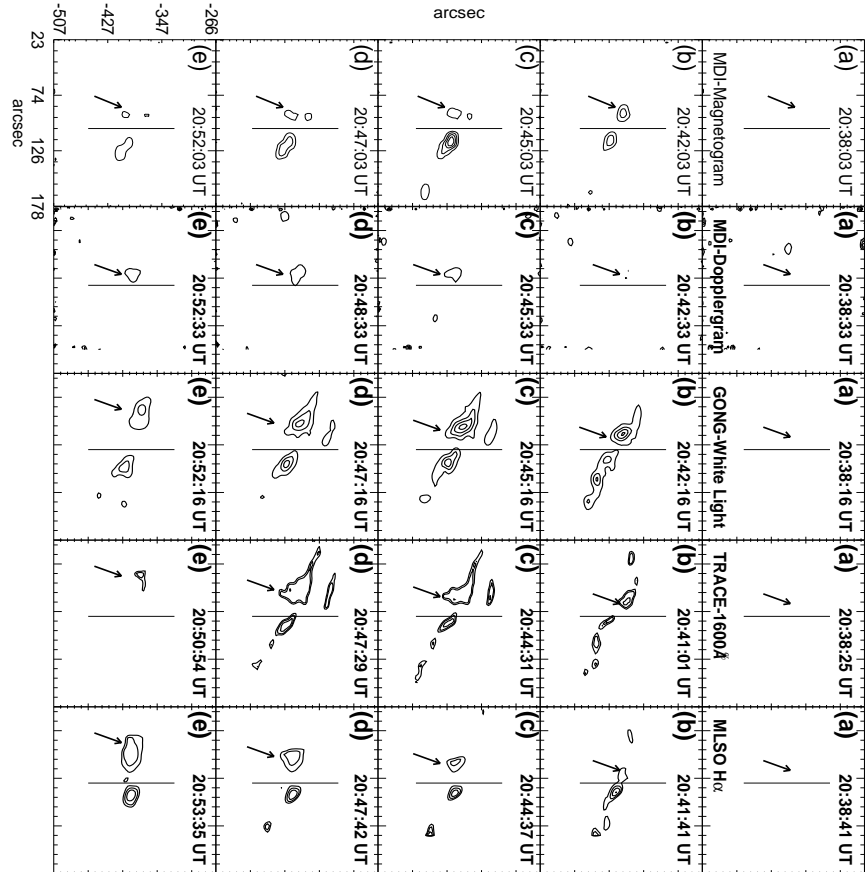


Figure 11. A mosaic of contours of different observations: magnetograms (MDI), Dopplergrams(MDI), white-light (GONG), TRACE -UV (1600Å) and H α (MLSO) (in columns from left to right) at different times of flare (X10/2B) of October 29, 2003. The rows corresponds to the time of observation during which MF and flare-kernels appeared simultaneously. Arrows have been drawn at the locations of MF and at corresponding positions in the flare-kernels. The solid line is the reference direction with respect to which MF and flare kernel motion were observed.

Distances of the flare kernels are determined by following the position of the maximum value within a feature of interest from the reference line NO along the line DX. The separation of various flare kernels are shown in Figure 11. In order to find the separation speeds of the flare kernels, we fitted straight lines (best fits) through the measured distances. The slopes of these fitted lines provided the respective velocities (Figure 12). The maximum distances and velocities are given in the Table 2. A similar trend in velocities of flare kernels is found as in the case of the flare of October 28, 2003; it generally increased from the upper to the lower atmospheric layer. However, the separation velocities are found be much smaller in this flare compared to the X17/4B flare of the previous day. Another

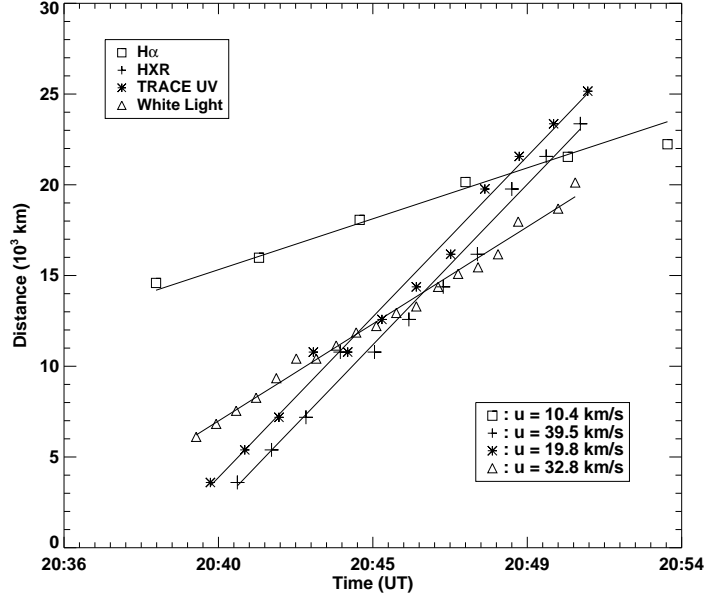


Figure 12. Distances of flare-kernels from the reference line NO, during 20:38:40 20:53:35UT for different observations: H α (MLSO), UV 1600Å(TRACE), white-light (GONG) and HXR (RHESSI). The measured distances are marked by symbols \square , $*$, \triangle and $+$ for H α , UV-1600Å, WL and HXR, respectively, while the solid lines represent the straight line fitting through the corresponding data points.

difference is that the magnetic and Doppler transients were found to remain approximately stationary during this flare. The distance and velocity profiles are also different from the event of October 28, 2003, where we could do a Boltzmann Sigmoid fitting as against the straight line fitting obtained for this flare. It is unlikely that velocity of flare kernels would remain constant throughout the flare duration, as it appears in this case. It is to note that flare kernels decayed in intensity, or fragmented, as they moved away from the reference line, and became generally difficult to follow beyond 20:51 UT. For H α kernel, however, there is an indication that the rate of change of separation decreased after this time.

Table 2. Maximum distances and velocities of the flare kernels.

S.N.	Data	Pixel Res. (arcsec)	Layer	Max. Dist. (Mm)	Max. Vel. (km s $^{-1}$)
1	USO-H α	0.4	Chr 2	23.5 \pm 0.3	10 \pm 5
2	HXR	4.0	Chr 2	28.3 \pm 0.9	33 \pm 6
3	TRACE 1600Å	0.5	TM 3	19.3 \pm 0.3	20 \pm 7
4	GONG WL	2.5	Pho 4	25.0 \pm 0.5	40 \pm 9

1 TR: Transition Region, 2 Chr: Chromosphere,

3 TM: Temperature Minimum, 4 Pho: Photosphere

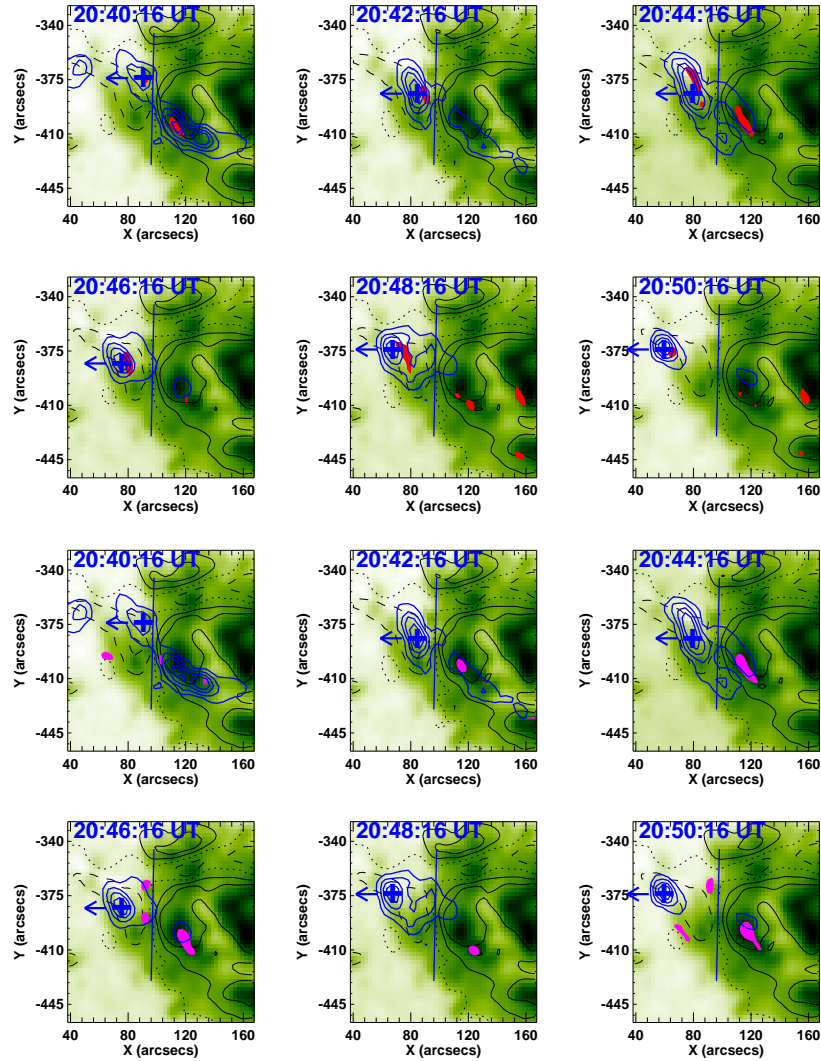


Figure 13. Time-sequence of white-light intensity maps (background half-tone green image) during the impulsive phase of the X10/2B flare - 20:40:16-20:50:16 UT on October 29, 2003. Superimposed dashed (solid) contours represent negative (positive) flux levels at ± 800 , ± 1500 gauss, and the dotted contours mark the magnetic neutral lines. RHESSI hard X-ray fluxes in the energy range 50-100 keV are overlaid at 20, 40, 60, 80% levels of the maximum value (blue contours). The red patches (top rows 1-2) show the positions of the WLF kernels, while the magenta patches (bottom rows 3-4) represent the magnetic transient features.

5.3. RHESSI Hard X-ray Sources and the White-light Flare of October 29, 2003

Figure 13 shows the temporal and spatial evolution of the enhanced white-light flare-kernels (red patches) observed in the GONG intensity maps (green half-tone images) obtained during the impulsive phase of the X10/2B flare of October 29,

2003 (top rows 1-2). Similarly, evolution of the magnetic transients (magenta patches) are shown with the same background images in the bottom rows (3-4). Blue contours represent the RHESSI HXR flux in the energy range 50-100 keV associated with the flare during its impulsive phase, i.e., 20:40:16-20:50:16 UT, at 20, 40, 60, 80% levels of the maximum flux. The central maxima of the hard X-ray source is marked by “+” sign in blue color. The solid blue line is drawn along the neutral line as a reference to measure the positions of various flare-kernels, observed to be moving in the direction of the arrow.

Corresponding to the white-light flare of October 29, 2003, Xu *et al.* (2004) obtained 1.56 μ m near-infrared images of the region \approx 50 km below the photosphere at the opacity minimum layer using the Dunn Solar Telescope at the National Solar Observatory/Sacramento Peak. These images indicated the extremely energetic activities associated with this flare, as only the most energetic electrons can penetrate this deep in the photosphere. Locations of GONG white-light kernels matched very well with the NIR continuum flare patches. However, not all these WLF kernels were associated with RHESSI HXR sources, as seen in Figure 13, (top rows 1-2). Also, locations of MFs, where sign-reversal anomaly appeared, did not conform well with these HXR sources, except at 20:40:16 UT (first two frames in row 3). Thereafter, the HXR source intensified at the opposite side of the neutral line, where the other part of the two-ribbon WLF kernel was located (top rows 1-2), but no magnetic transient feature (magenta patches in rows 3-4) was present. Interestingly, we note that the strong HXR source (and the WLF kernel) which intensified at this side of the neutral line was located in a weak field region, in disagreement with the suggestion of Qiu and Gary (2003). On the other hand, the magnetic transient feature was observed over the stronger field region of the positive polarity umbra, generally associated with WLF kernel, but without HXR source. This behaviour is in contrast with the white-light flare of October 28, 2003, and also in contradiction with the earlier suggestions about the association of sign reversal phenomenon with HXR sources.

6. Discussions and Conclusions

We observed moving transients and sign reversals of magnetic polarity at some locations of NOAA 10486 during the impulsive phases of both the white light flares of October 28 and 29, 2003. Along with the magnetic transients, comparatively fainter Doppler transients were also discernible during this period. The magnetic and velocity transients were observed to be particularly well correlated. The locations of moving transients were also the locations where sign reversals in magnetic polarity and velocity occurred.

The two flares were quite different in their energetics - the October 28 flare was X17/4B, while, the October 29 flare was X10/2B. They occurred at topologically different locations within the active region. We have attempted to examine properties and relationship of the observed features and flare kernels in various atmospheric layers for the two events. There are some interesting questions related to these observed transients: What physical process caused the moving magnetic and velocity transients? Is there any relationship between the moving transients, HXR sources and the flare kernels?

The GONG and MDI instruments use the same spectral line (Ni I 6768Å), but different principles of observations (Harvey 2008, private communication, see Appendix). Nevertheless, observed motions of the magnetic, velocity and intensity fields obtained from both instruments were found to be similar. Sign reversals in magnetic and velocity fields were detected by both the instruments during the impulsive phase of solar flares of October 28 and 29, 2003. In some cases, these transients occurred near the cooler umbral/penumbral sites of the active region NOAA 10486, but there were also several exceptions.

In the case of the X17/2B flare of October 28, 2003, we found two locations of magnetic transients associated with sign reversals in magnetic polarity (and Doppler velocity). A part of the magnetic feature moved toward the following (positive) umbra from the neutral line and the other developed within the leading (negative) umbra. These differed in their basic characteristics- (i) one location of sign reversal was nearly stationary, observed in strong magnetic field of the leading, negative polarity umbra. Both, HXR foot-point and WLF kernel were associated with this location of sign reversal, (ii) another location of sign reversal was observed in a weak field area, moved rapidly toward strong field of the positive (following) polarity umbra, had better association with HXR as compared to some WLF kernels.

On the other hand, magnetic and Doppler transients observed on October 29, 2003 were nearly stationary during the course of the X10/2B flare. The locations of magnetic transients, where sign-reversal anomaly appeared, did not conform well with the HXR sources. Interestingly, we observed a strong HXR source (and WLF kernel) in weak field region without sign reversal anomaly. On the other hand, there was WLF kernel but no HXR source associated with the magnetic transient observed over the strong field of the positive polarity umbra. This is in contrast with the HXR-magnetic anomaly relation observed for the white-light flare of October 28, 2003, and also contradicts the earlier suggestions of Qiu and Gary (2003) about the association of HXR sources with polarity sign reversal phenomenon.

We found that magnetic/velocity transients generally followed the usual behaviour of separation of flare-kernels observed in two-ribbon flares. Let us first discuss the motion of magnetic transients observed during the flare of October 28, 2003. There was an interesting trend in maximum separation attained for the flare-kernels observed in successively lower layers of solar atmosphere: the shortest, i.e., ≈ 15 Mm at the transition layer as observed in UV 284Å (TRACE), increasing to ≈ 20 Mm at the chromosphere (USO-H α) and ≈ 28 Mm in the temperature minimum region and the photosphere (UV 1600Å TRACE, and GONG & MDI photospheric data). This trend is consistent with the classical flare model of an expanding loop structure with foot-points anchored in the lower atmosphere. The HXR feature also showed separation of ≈ 23 Mm, nearly the same as the separation observed in chromospheric H α . This is consistent with the formation of HXR sources somewhere in the lower chromospheric layer. The magnetic and doppler transients, on the other hand, showed a larger separation of ≈ 29 Mm which matched the value obtained for the photospheric WLF kernels.

Furthermore, we found that the flare-kernels separated faster in the lower atmosphere (the temperature minimum region and the photosphere) with velocity

of 45-50 km/s as compared to that in the upper atmosphere, i.e., 38 km/s at the chromosphere, and 29 km/sec at the even higher transition region. However, the separation velocities for the X10/2B flare kernels were found to be much smaller as compared to the X17/4B flare of the previous day, i.e., October 28, 2003.

Ding, Qiu, and Wang (2002), using atmospheric model showed that the line inversion occurs near sunspot penumbral area if electron density rises significantly. It is to note that a significant rise in the electron density was found during the impulsive phase of the flare of October 28, 2003 (Klassen *et al.*, 2005), which is also consistent with the RHESSI-HXR observations. Therefore, occurrence of the moving transients appears to be related to the line profile changes due to the process associated with the electron-beams, and not due to any real changes in the photospheric magnetic and velocity fields. However, no clear conclusions are discernible for the X10/2B flare of October 29, 2003. Also, away from these features permanent change in magnetic fluxes from the pre- to post-flare phases have been reported that do not seem to be affected by the WLF or HXR related effects (Ambastha, 2007).

It is interesting to note that the observed flare-kernels and moving transients associated with these events possessed large velocities. This is as expected due to the large magnetic energy stored in the active region giving rise to these energetic super-flares. The particles were energised and thermal conduction propagated along the reconnected loops from the coronal reconnection site toward the foot-points. As they precipitated into different layers of the solar atmosphere, flare kernels formed on either side of the magnetic neutral line. The large velocity of the flare kernels is due to the outward conduction of the energy from the neutral line in the corresponding layers.

Finally, the answer to the question of correlation of the moving magnetic transients (or polarity reversals) with HXR sources or WLF kernels still appears to be rather ambiguous, as we did not find a clear association of the magnetic anomaly with either the HXR or with the WLF kernels.

Appendix

- *Principle of SOHO/MDI Observations:* The MDI instrument on board SOHO uses photospheric absorption line at Ni I 6767.8Å. The center of the wavelength bandpass is tunable in steps of about 8 mÅ over a range of 377 mÅ centered on the Ni I. The width of the bandpass is fixed at 94 mÅ. The incident light can be in any of four polarization states: s-wave, p-wave, right-hand circular, and left-hand circular. Camera readout time limits the rate at which successive filtergrams can be taken to about 1 every 3 seconds. They all involve sets of filtergrams at five fixed wavelengths separated by 75 mÅ, denoted by I_0 , I_1 , I_2 , I_3 , and I_4 . The filtergrams are combined on board by an image processor to produce the secondary observables, which can then be sampled, binned, and/or filtered depending on the observing program. The Doppler shift is calculated as a tabulated nearly linear function of the filtergram difference ratios: $r_1 = (I_1 + I_2 - I_3 - I_4)/(I_1 - I_3)$ and $r_2 = (I_1 + I_2 - I_3 - I_4)/(I_4 - I_2)$. The per-pixel measurement uncertainty

for a one-minute measurement is equivalent to 20 m/s. The Zeeman splitting is determined by the difference between the Doppler shifts calculated from the filtergram components taken separately in right-hand and left-hand circularly polarized light. The per-pixel measurement uncertainty for a two-minute measurement is equivalent to 20 Gauss.

- *Principle of GONG Observations:* The measurement principle of GONG is more complicated than MDI. The main reason is that on the ground we have to contend with rapidly changing atmospheric seeing conditions which would make a lot of noise using the MDI method. The principle used in GONG is phase shift interferometry. The instrument makes 60 images per second of the sun as transmitted using a 0.7Å pass band filter centered on the 6767.8Å Ni I spectrum line. An interferometer produces a sinusoidal transmission function of wavelength across the passband having a period of about 0.3Å. This transmission function is swept in wavelength smoothly at a rate of 1/3 fringe per 1/60 second camera frame time in synchronism with the camera. Thus we get three images of the sun in 1/20 second that have different intensities (are modulated) depending on the position of the transmission profile relative to the solar spectrum line. From these three images it is easy to derive the phase of the intensity modulation, the strength of the modulation and the average intensity. The phase depends on the Doppler shift of the spectrum line and is therefore the basic velocity information produced by the GONG instrument. Regarding the magnetic field, it is done as follows. We integrate for one second using right circularly polarized (RCP) input light. Then a liquid crystal modulator changes retardation so that left circularly polarized (LCP) light images are integrated separately for the next second and so on until 60 seconds total integration is reached. The integrated RCP images produce one velocity image and the integrated LCP images a second velocity image. The difference between them is the longitudinal Zeeman splitting (magnetic field) plus some noise from the evolution of the real velocity field over one second and image differences caused by atmospheric seeing.

Acknowledgements We are thankful to J. Harvey, NSO, for communicating the detailed description of the principle of GONG observations and its inter-comparison with MDI.

This work utilizes data obtained by the Global Oscillation Network Group (GONG) project, managed by the National Solar Observatory which is operated by AURA Inc., under a cooperative agreement with the National Science Foundation. The GONG data were acquired by instruments operated by the Big Bear Solar Observatory, High Altitude Observatory, Learmonth Solar Observatory, Udaipur Solar Observatory, Instituto de Astrofisico de Canarias and Cerro Tololo Inter-American Observatory.

This work utilises data from the Solar Oscillations Investigation/ Michelson Doppler Imager (SOI/MDI) on the Solar and Heliospheric Observatory (SOHO). SOHO is a project of international cooperation between ESA and NASA. MDI is supported by NASA grants NAG5-8878 and NAG5-10483 to Stanford University.

We would like to express thanks for the H α data to Mauna Loa Solar Observatory (MLSO). MLSO is operated by the High Altitude Observatory (HAO), a

division of the National Center for Atmospheric Research (NCAR), and funded by the National Science Foundation (NSF).

This work also utilises data obtained by RHESSI.

References

Abramenko, V.I., Baranovsky, E.A.: 2004, *Solar Phys.* **220**, 81. doi:10.1023/B:sola.0000023432.42145.b0.

Ambastha, A.: 2007, *Sun and Geosphere* **2**, 13.

Ambastha, A.: 2007, *Bul. Astron. Soc. India* **35**, 419.

Ambastha, A.: 2008, *J. Astrophys. Astron.* **29**, 93. doi:10.1007/s12036-008-0012-3.

Ambastha, A., Basu, S., Antia, H.M.: 2003, *Solar Phys.* **218**, 151. doi:10.1023/B:SOLA.0000013043.45512.20.

Ambastha, A., Hagyard, M.J., West, E.A.: 1993, *Solar Phys.* **148**, 277. doi:10.1007/BF00645091.

Ambastha, A., Basu, S., Antia, H.M., Bogart, R.S.: 2004, In: Danesy, D. (ed.) *SOHO 14 Helio- and Asteroseismology: Towards a Golden Future, ESA Special Publication* **559**, 293.

Brown, J.C.: 1971, *Solar Phys.* **18**, 489. doi:10.1007/BF00149070.

Bruls, J.H.M.J.: 1993, *Astron. Astrophys.* **269**, 509.

Chen, J., Wang, H., Zirin, H., Ai, G.: 1994, *Solar Phys.* **154**, 261. doi:10.1007/BF00681099.

Ding, M.D., Fang, C.: 1989, *Astron. Astrophys.* **225**, 204.

Ding, M.D., Qiu, J., Wang, H.: 2002, *Astrophys. J. Lett.* **576**, 83. doi:10.1086/343103.

Domea, A.C., Lindsey, C.: 2005, *Astrophys. J.* **630**, 1168. doi:10.1086/432155.

Edelman, F., Hill, F., Howe, R., Komm, R.: 2004, In: Danesy, D. (ed.) *SOHO 14 Helio- and Asteroseismology: Towards a Golden Future, ESA Special Publication* **559**, 416.

Emslie, A.G.: 1978, *Astrophys. J.* **224**, 241. doi:10.1086/156371.

Fletcher, L., Hudson, H.: 2001, *Solar Phys.* **204**, 69. doi:10.1023/A:1014275821318.

Giovanelli, R.G.: 1939, *Astrophys. J.* **89**, 555. doi:10.1086/144081.

Hagyard, M.J., Stark, B.A., Venkatakrishnan, P.: 1999, *Solar Phys.* **184**, 133.

Handy, B.N., Acton, L.W., Kankelborg, C.C., Wolfson, C.J., Akin, D.J., Bruner, M.E., Caravalho, R., Catura, R.C., Chevalier, R., Duncan, D.W., Edwards, C.G., Feinstein, C.N., Freeland, S.L., Friedlaender, F.M., Hoffmann, C.H., Hurlburt, N.E., Jurcevich, B.K., Katz, N.L., Kelly, G.A., Lemen, J.R., Levay, M., Lindgren, R.W., Mathur, D.P., Meyer, S.B., Morrison, S.J., Morrison, M.D., Nightingale, R.W., Pope, T.P., Rehse, R.A., Schrijver, C.J., Shine, R.A., Shing, L., Strong, K.T., Tarbell, T.D., Title, A.M., Torgerson, D.D., Golub, L., Bookbinder, J.A., Caldwell, D., Cheimets, P.N., Davis, W.N., Deluca, E.E., McMullen, R.A., Warren, H.P., Amato, D., Fisher, R., Maldonado, H., Parkinson, C.: 1999, *Solar Phys.* **187**, 229. doi:10.1023/A:1005166902804.

Harvey, J.: 1986, In: Deinzer, W., Knölker, M., Voigt, H.H. (eds.) *Small Scale Magnetic Flux Concentrations in the Solar Photosphere*, 25.

Harvey, J., Abdel-Gawad, K., Ball, W., Boxum, B., Bull, F., Cole, J., Cole, L., Colley, S., Dowdney, K., Drake, R., Dunn, R., Duval, T., Farris, D., Green, A., Hartlmeier, R., Harvey, J., Hubbard, R., Jackson, P., Kucera, D., Miller, C., Miller, D., Petri, A., Poczulp, G., Schwitters, J., Simmons, J., Smartt, R., Streander, G., Vaughn, F., Wiborg, P., GONG Instrument Development Team: 1988, In: Rolfe, E.J. (ed.) *Seismology of the Sun and Sun-Like Stars, ESA Special Publication* **286**, 203.

Hudson, H.S., Acton, L.W., Hirayama, T., Uchida, Y.: 1992, *Pub. Astron. Soc. Japan* **44**, 77.

Hurford, G.J., Schmahl, E.J., Schwartz, R.A., Conway, A.J., Aschwanden, M.J., Csillaghy, A., Dennis, B.R., Johns-Krull, C., Krucker, S., Lin, R.P., McTiernan, J., Metcalf, T.R., Sato, J., Smith, D.M.: 2002, *Solar Phys.* **210**, 61. doi:10.1023/A:1022436213688.

Klassen, A., Krucker, S., Kunow, H., Müller-Mellin, R., Wimmer-Schweingruber, R., Mann, G., Posner, A.: 2005, *Journal of Geophysical Research (Space Physics)* **110**, 9. doi:10.1029/2004JA010910.

Kosovichev, A.G.: 2006, *Solar Phys.* **238**, 1. doi:10.1007/s11207-006-0190-6.

Kosovichev, A.G., Zharkova, V.V.: 1998, *Nature* **393**, 317. doi:10.1038/30629.

Kosovichev, A.G., Zharkova, V.V.: 2001, *Astrophys. J. Lett.* **550**, 105. doi:10.1086/319484.

Lee, J., Gary, D.E., Qiu, J., Gallagher, P.T.: 2002, *Astrophys. J.* **572**, 609. doi:10.1086/340311.

Lin, R., Dennis, B., Benz, A., Harvey, J., Engvold, O., Švestka, Z.: 2002, *Solar Phys.* **210**, 1. doi:10.1007/s11207-004-0827-2.

Machado, M.E., Avrett, E.H., Vernazza, J.E., Noyes, R.W.: 1980, *Astrophys. J.* **242**, 336. doi:10.1086/158467.

Maurya, R.A., Ambastha, A.: 2008, *J. Astrophys. Astron.* **29**, 103. doi:10.1007/s12036-008-0013-2.

Metcalf, T.R., Alexander, D., Hudson, H.S., Longcope, D.W.: 2003, *Astrophys. J.* **595**, 483. doi:10.1086/377217.

Narayan, R., Nityananda, R.: 1986, *Ann. Rev. Astron. Astrophys.* **24**, 127. doi:10.1146/annurev.aa.24.090186.001015.

Neidig, D.F., Kane, S.R.: 1993, *Solar Phys.* **143**, 201. doi:10.1007/BF00619106.

Patterson, A.: 1984, *Astrophys. J.* **280**, 884. doi:10.1086/162063.

Patterson, A., Zirin, H.: 1981, *Astrophys. J. Lett.* **243**, 99. doi:10.1086/183451.

Qiu, J., Gary, D.E.: 2003, *Astrophys. J.* **599**, 615. doi:10.1086/379146.

Qiu, J., Lee, J., Gary, D.E., Wang, H.: 2002, *Astrophys. J.* **565**, 1335. doi:10.1086/324706.

Rust, D.M., Hegwer, F.: 1975, *Solar Phys.* **40**, 141. doi:10.1007/BF00183158.

Scherrer, P.H., Bogart, R.S., Bush, R.I., Hoeksema, J.T., Kosovichev, A.G., Schou, J., Rosenberg, W., Springer, L., Tarbell, T.D., Title, A., Wolfson, C.J., Zayer, I., MDI Engineering Team: 1995, *Solar Phys.* **162**, 129. doi:10.1007/BF00733429.

Schrijver, C.J., Title, A.M., Berger, T.E., Fletcher, L., Hurlburt, N.E., Nightingale, R.W., Shine, R.A., Tarbell, T.D., Wolfson, J., Golub, L., Bookbinder, J.A., Deluca, E.E., McMullen, R.A., Warren, H.P., Kankelborg, C.C., Handy, B.N., de Pontieu, B.: 1999, *Solar Phys.* **187**, 261. doi:10.1023/A:1005194519642.

Skilling, J., Bryan, R.K.: 1984, *Mon. Not. Roy. Astron. Soc.* **211**, 111.

Sudol, J.J., Harvey, J.W.: 2005, *Astrophys. J.* **635**, 647. doi:10.1086/497361.

Venkatakrishnan, P., Kumar, B., Uddin, W.: 2008, *Mon. Not. Roy. Astron. Soc.* **387**, 69. doi:10.1111/j.1745-3933.2008.00487.x.

Vernazza, J.E., Avrett, E.H., Loeser, R.: 1981, *Astrophys. J. Sup. Ser.* **45**, 635. doi:10.1086/190731.

Wang, H.: 2006, *Astrophys. J.* **649**, 490. doi:10.1086/506320.

Wang, H., Varsik, J., Zirin, H., Canfield, R.C., Leka, K.D., Wang, J.: 1992, *Solar Phys.* **142**, 11. doi:10.1007/BF00156630.

Xu, Y., Cao, W., Liu, C., Yang, G., Qiu, J., Jing, J., Denker, C., Wang, H.: 2004, *Astrophys. J. Lett.* **607**, 131. doi:10.1086/422099.

Zharkova, V.V., Zharkov, S.I.: 2007, *Astrophys. J.* **664**, 573. doi:10.1086/518731.

Zirin, H., Tanaka, K.: 1981, *Astrophys. J.* **250**, 791. doi:10.1086/159429.